Boundary Integral Equations in Linearly Graded Media

Brad Nelson

Senior Thesis
Department of Mathematics
Dartmouth College

Advisor: Alex Barnett

May 28, 2013

Abstract

Boundary integral equations (BIEs) are a popular method for numerical solution of Helmholtz boundary value problems in a piecewise-uniform medium. We generalize BIEs for the first time to a continuously-graded medium in two dimensions, where the square of the wavenumber varies linearly with one coordinate. Using these techniques, we gain a significant advantage over the alternative finite element/finite difference schemes for solving scattering problems in this type of medium. Applications include acoustics and optics with thermal/density/index gradient. We present an evaluation scheme for the fundamental solution using contour integrals, and give examples of interior/exterior Dirichlet problems, as well as high-frequency scattering problems.

Acknowledgements

First and foremost, I would like to thank Professor Barnett for his mentorship and assistance throughout this project, as well as his guidance in my attempts to navigate the world of mathematics.

A portion of this research was completed during Spring term 2012, and was made possible through a grant from the Paul K. Richter and Evalyn E. Cook Richter Memorial Fund.

I would also like to thank the Neukom Institute at Dartmouth College for providing a travel grant to present a version of this work at the SIAM CSE 2013 conference in a student poster session.

1 Introduction

Boundary value problems (BVPs) arise when modeling many kinds of natural phenomena, including electromagnetics, acoustics, and optics. A BVP seeks a function that satisfies a partial differential equation (PDE) within a domain, and that satisfies boundary conditions along the boundary of the domain. If we let $\mathcal{L}$ be a second-order partial-differential operator, we formulate a boundary value problem for a function u as

$$\begin{cases} \mathcal{L}u = 0 & \text{in } \Omega \\ u = f & \text{on } \partial\Omega \end{cases} \tag{1}$$

where Ω is an interior or exterior domain, $\partial\Omega$ denotes its boundary, and f is a given function $f : \partial\Omega \to \mathbb{R}$. Boundary data that requires $u = f$, as above, is known as Dirichlet boundary data. Boundary data that matches the normals derivative of u to a function, $u_n = f$, is known as Neumann boundary data. Mixed boundary data requires $u + \beta u_n = f$ for some $\beta \in \mathbb{C}$. In interior problems, Ω is a simply-connected, bounded domain. In exterior problems, including scattering problems, the domain's complement is simply-connected and bounded. In this thesis, we primarily consider both interior and exterior problems with Dirichlet boundary data.

Two common examples of boundary value problems are the Laplace and Helmholtz problems. Both equations are useful in describing electromagnetic, acoustic, and optical phenomena. A Helmholtz BVP, which describes a wave function u, is formulated as

$$\begin{cases} (\Delta + k^2(\mathbf{x}))u = 0 & \text{in } \Omega \\ u = f & \text{on } \partial\Omega \end{cases} \tag{2}$$

where $\mathbf{x} = (x_1, x_2, \dots)$, $k(\mathbf{x})$ is the location-dependent wavenumber of u, and Δ is the Laplacian operator,

$$\Delta = \sum_i \frac{\partial^2}{\partial x_i^2} \tag{3}$$

The Laplace equation is similar to the Helmholtz, except $k^2 = 0$ everywhere.

Classic techniques for solving BVPs numerically are the finite element and finite difference methods. Both methods involve a discretization of the domain of the problem, and matching conditions at each point. For instance, if we are interested in solving a BVP in the unit square using the finite difference method, then the system will be discretized into $n \times n$ points, resulting in n^2 unknowns. This results in an $n^2 \times n^2$ linear system that is sparse, but poorly conditioned, demanding complicated preconditioners if an iterative solver is used [10]. Additionally, solving exterior problems using these methods require artificial conditions, such as perfectly matched layers (PMLs) to handle radiation conditions.

Boundary integral equations (BIEs) are a popular alternative to these classical discretization schemes for Helmholtz and Laplace BVPs in (piecewise) uniform media (meaning that $k(\mathbf{x})$ is piecewise constant in the domain). BIEs reduce the problem to solving a linear system on the boundary of the domain, so the size of the problem grows with the perimeter of the domain, rather than its volume. Additionally, BIEs have the advantage of being well-conditioned, allowing for accurate solution of the linear system using standard linear algebraic techniques, and methods such as the fast

multipole method (FMM) allow for iterative solution in near-linear time. BIEs also have the advantage of being able to solve exterior BVPs without the use of PMLs.

The particular BVP that is investigated in this thesis is a variation of the Helmholtz equation where $k^2(\mathbf{x})$ varies linearly in one coordinate of the domain:

$$\begin{cases} (\Delta + x_2 + E)u = 0 & \text{in } \Omega \\ u = f & \text{on } \partial\Omega \end{cases} \tag{4}$$

Because of the linear term x_2, we refer to this as the linear Helmholtz equation. Note that generally, a PDE with a linear dependence of the form $k^2(\mathbf{x}) = \mathbf{a} \cdot \mathbf{x} + E$ can be transformed into equation (4) through a change of variables in the domain. This equation describes natural phenomena such as acoustics in a temperature/density gradient (particularly underwater acoustics), optics in a medium with a linearly graded index of refraction, and electromagnetic waves or a quantum particle in a linear potential.

2 Boundary Integral Equations

2.1 Overview

An integral equation is an equation

$$b(x) = \int_a^b K(x,y)\tau(y)\,dy$$

Where b and K are given, and we are trying to solve for the function τ. This is the continuous analog of solving a linear system

$$\mathbf{b} = \mathbf{K}\boldsymbol{\tau}$$

for $\boldsymbol{\tau}$. We refer to $K(x,y)$ as the kernel of the integral equation.

The basic idea of BIEs are to use a function, called a fundamental solution, that satisfies the PDE everywhere but a point, called the source of the fundamental solution, as the kernel of an integral equation. This formulation obeys jump relations, which allow for boundary data to be matched. By weighting fundamental solution with a density function along the boundary of the domain, we satisfy the PDE and the boundary conditions.

When we discretize the system, as shown in figure 1 this amounts to taking a linear combination of fundamental solutions, whose sources lie along the boundary of the domain. Since we are considering a linear PDE, a linear combination of fundamental solutions will satisfy the PDE everywhere but where the sources lie. Since the sources all lie on the boundary of the domain, the linear combination of fundamental solutions will satisfy the PDE inside the domain. In effect, we are simply solving for a set of weights for our discrete set of fundamental solutions in order to match boundary values, since satisfying the PDE is already guaranteed.

2.2 The Fundamental Solution

A fundamental solution is a function that satisfies a PDE everywhere except for a point

Definition 1. *Let $\mathcal{L}_x$ be a second-order differential operator acting on the $\mathbf{x}$ variable only. Then $\Phi(\mathbf{x},\mathbf{y})$ is a fundamental solution of $\mathcal{L}_x$ if $\mathcal{L}_x\Phi(\mathbf{x},\mathbf{y}) = \delta_{\mathbf{y}}(\mathbf{x})$, where δ_y is the Dirac delta distribution at point $\mathbf{y}$. We refer to $\mathbf{y}$ as the source of the fundamental solution, and $\mathbf{x}$ as the the target.*

For exterior BIEs, we seek a radiative fundamental solution. Garabedian [6] offers an alternate, equivalent, definition

Proposition 1. *[6] (5.4) Let $\mathcal{L}_x$ be a second-order general elliptic operator. Then any fundamental solution for $\mathcal{L}_x$ is of the form*

$$\Phi(\mathbf{x},\mathbf{y}) = A(\mathbf{x},\mathbf{y})\log\frac{1}{|\mathbf{r}|} + B(\mathbf{x},\mathbf{y}) \tag{5}$$

Where $\mathbf{r} = \mathbf{x} - \mathbf{y}$, and A, B are continuous functions if the coefficients of the operator are continuous. Furthermore

$$\lim_{\mathbf{r}\to\mathbf{0}} A(\mathbf{x},\mathbf{y}) = 1/2\pi$$

That is, that the singularity at $\mathbf{x} = \mathbf{y}$ is logarithmic.

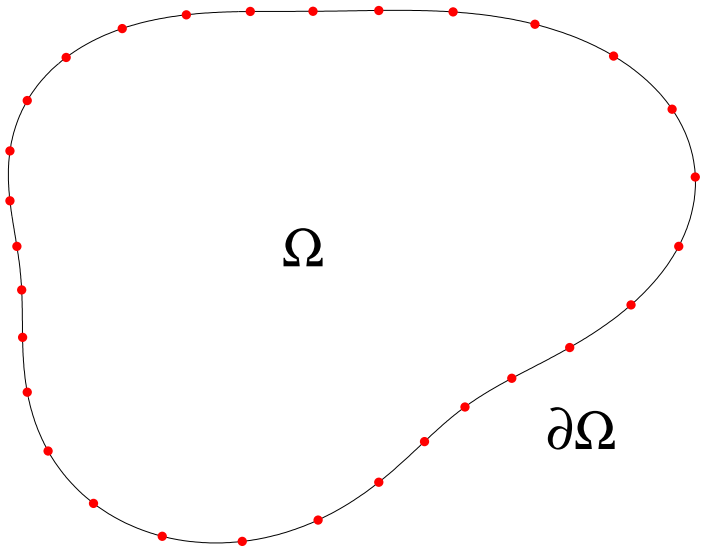

Figure 1: Example of discretization for an interior boundary value problem using boundary integral equations. We place fundamental solutions with sources at the red dots, and solve for their weights.

A physical interpretation of the fundamental solution is that it is a point source (such as an electric pole) in a potential. The fundamental solution for the Laplace equation in two dimensions is:

$$\Phi(\mathbf{x}, \mathbf{y}) = \frac{1}{2\pi} \log\left(\frac{1}{|\mathbf{r}|}\right) \tag{6}$$

The fundamental solution for the Helmholtz equation in a homogenous medium (constant k) in two dimensions is:

$$\Phi(\mathbf{x}, \mathbf{y}) = \frac{i}{4} H_0^{(1)}(k|\mathbf{x} - \mathbf{y}|) \tag{7}$$

We seek a fundamental solution for the operator of interest (equation (4)) in two dimensions.

Proposition 2. *[3, 11] A radiative fundamental solution for $\mathcal{L}_x = \Delta + x_2 + E$ in two dimensions is given by*

$$\Phi(\mathbf{x}, \mathbf{y}) = -\frac{1}{4\pi} \int_{-\infty}^{\infty} \exp i\Big[\frac{|\mathbf{x} - \mathbf{y}|^2}{4} e^{-s} + (\frac{1}{2}x_2 + \frac{1}{2}y_2 + E)e^s - \frac{1}{12}e^{3s}\Big]\, ds \tag{8}$$

Sketch of Proof: [3, 11] We start with the definition of our fundamental solution,

$$(\Delta + x_2 - E)\Phi = \delta_y(\mathbf{x})$$

Then we take a Fourier transform relating the E variable to t

$$(\Delta + x_2 + i\partial_t)\widetilde{\Phi} = \delta_y(\mathbf{x})\delta(t)$$

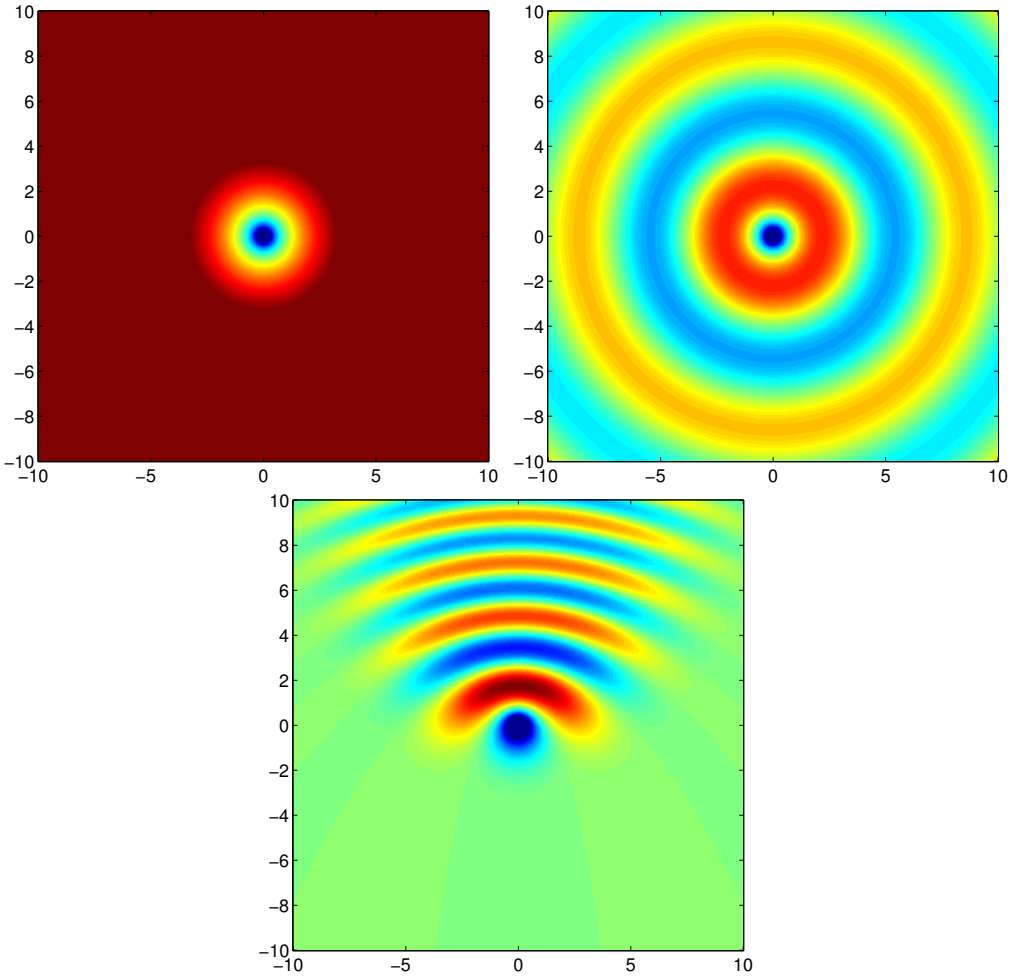

Figure 2: Fundamental solutions in the (x_1, x_2) plane, with $\mathbf{y} = (0, 0)$. Top left: fundamental solution for Laplace's equation (6). Top right: fundamental solution for the Helmholtz equation ($k = 1$) (7). Bottom: fundamental solution for the linear Helmholtz equation ($E = 1$) (8).

This is equivalent to a time-dependent Schrödinger equation in a linear potential, which can be solved using yet another Fourier transform in the spatial dimensions, eventually giving the above result. This contrasts to the usual frequency-time connection used in the wave equation.

Since this fundamental solution is derived from the Fourier transform of a causal greens function for the time-dependent Schrödinger equation, we believe that it is the physically relevant greens function for the time-harmonic case, meaning that it is an outwardly radiative solution. However, no formal radiation condition exists in the literature.

In section 4, we present numerical algorithms to evaluate this fundamental solution.

2.2.1 Physical Interpretation

First, we note the connection of our wave equation to the Schrödinger equation, which describes the wave function of a quantum particle. The linear Helmholtz equation:

$$(\Delta + x_2 + E)u = 0$$

becomes

$$[-\Delta/2 + (-x_2/2 - E/2)]u = 0$$

when divided by -2. This is the (dimensionless) time-independent Schrödinger equation

$$Hu = [-\Delta/2 + V(\mathbf{x})]u(\mathbf{x}) = 0$$

With potential energy $V(x) = -x_2/2 - E/2$.

The fundamental solution is thus the solution to the Schrödinger equation with a point-source at $\mathbf{y}$. This corresponds to the interference pattern of particles emanating from the source in all directions. In order to simulate this, we can start particles at the source with kinetic energy $E/2$, and subject them to a force of strength $1/2$ in the $+x_2$ direction.

As seen in fig. 3, the fundamental solution dies off in areas where the particles are "classically forbidden," and follows the parabolic shape of the classical trajectories.

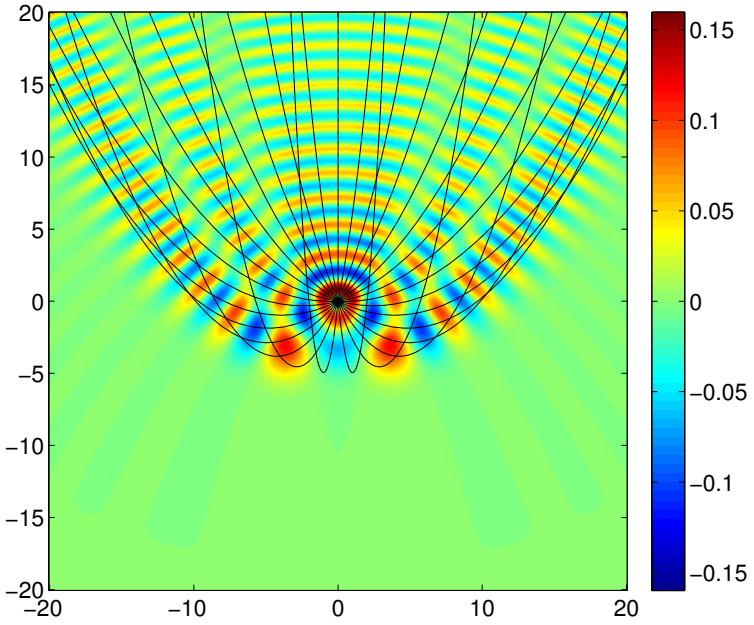

Figure 3: Trajectories of classical particles emanating from the origin, $E = 5$, superimposed on the fundamental solution for the same E.

2.3 Jump Relations

As mentioned previously, one of the reasons that the fundamental solution is useful is that it obeys certain relations at the source that allow for matching of boundary conditions.

Definition 2. *Given a fundamental solution $\Phi(\mathbf{x}, \mathbf{y})$ and a domain Ω we define the following integral operators:*

$$(\mathcal{S}\sigma)(\mathbf{x}) = \int_{\partial\Omega} \Phi(\mathbf{x}, \mathbf{y})\sigma(\mathbf{y})\, dy \tag{9}$$

$$(\mathcal{D}\tau)(\mathbf{x}) = \int_{\partial\Omega} \frac{\partial\Phi(\mathbf{x}, \mathbf{y})}{\partial\mathbf{n}(\mathbf{y})}\tau(\mathbf{y})\, dy \tag{10}$$

We refer to $\mathcal{S}$ as the "single layer representation" and we refer to $\mathcal{D}$ as the "double layer representation." We define the boundary integral operators

$$(S\sigma)(\mathbf{x}) = (\mathcal{S}\sigma)(\mathbf{x}), x \in \partial\Omega \tag{11}$$

As the restriction of $(\mathcal{S}\sigma)$ to $\partial\Omega$, and

$$(D\tau)(\mathbf{x}) \tag{12}$$

principle value integral of (10) with $\mathbf{x}$ on the boundary $\partial\Omega$. We refer to these two boundary integral operators as the "single layer operator" and "double layer operator" respectively.

Theorem 1. *Let $\partial\Omega$ be of class C^2, density σ be continuous. Define*

$$u(\mathbf{x}) = (\mathcal{S}\sigma)(\mathbf{x}) \tag{13}$$

then $u(\mathbf{x})$ is uniformly continuous in $\mathbb{R}^2$.

Theorem 2. *Let $\partial\Omega$ be of class C^2, density τ be continuous. Define*

$$v(\mathbf{x}) = (\mathcal{D}\tau)(\mathbf{x}) \qquad \mathbf{x} \in \mathbb{R}^2 - \partial\Omega \tag{14}$$

Then

$$v_{\pm}(\mathbf{x}) = (D\tau)(\mathbf{x}) \pm \tau(\mathbf{x})/2 \qquad \mathbf{x} \in \partial\Omega \tag{15}$$

where

$$v_{\pm}(\mathbf{x}) = \lim_{h\to 0^+} v(\mathbf{x} \pm h\mathbf{n}(\mathbf{x}))$$

For proof of Theorems 1 and 2 for the Laplace and homogeneous Helmholtz equations, we refer to [4].

To sketch a proof for the linear Helmholtz case, we note that Proposition 1 gives us that the fundamental solution (8) is a continuous perturbation of the fundamental solution of the Laplace equation (6), and has an identical singularity at the source. Following the proof of the jump relations in Garabedian [6] 5.1, we form a contour encircling the source of an isolated fundamental solution. Since the fundamental solution locally resembles the fundamental solution for Laplace's equation, as we shrink the radius of the contour, the integral over the contour for both fundamental solutions agree. Since the evaluation of this integral gives the jump relations, we see that the jump relations hold for the linear Helmholtz fundamental solution.

2.4 Integral Equations

Now, since we seek a solution to a Dirichlet BVP (1), we see that the jump relations give us an easy solution. We simply need to find a single layer density $\sigma(\mathbf{x})$ or double layer density $\tau(\mathbf{x})$ such that $S\sigma$ or $(D \pm 1/2)\tau$ agrees with the given boundary data. The single-layer operator gives a Fredholm integral equation of the first kind, which is subject to ill-conditioning, making it difficult to solve accurately. But, the double layer operator gives a Fredholm integral equation of the second kind, which is well-conditioned, so we will focus on this formulation of the problem.

For an interior Dirichlet Problem, it suffices to use the double layer operator. However, exterior/scattering problems are subject to spurious resonances. To avoid this problem, we use the kernel

$$D - i\eta S \tag{16}$$

which also provides a second-kind formulation:

$$(1/2 + D - i\eta S)\tau = f \tag{17}$$

We call this the combined field integral equation [5]. Generally, we take $\eta \approx k$ for the homogenous Helmholtz equation. Since the wavenumber varies over the domain in the linear Helmholtz case, we will take $\eta = \sqrt{E}$.

3 Nyström Method & Quadrature

In the previous section, we outlined the formulation of a boundary integral equation. However, to solve such problems numerically, we must discretize the boundary of the domain, and use quadrature rules to evaluate the integral. This section contains a discussion of the discretization of the integral and a discussion of dealing with the singular operator.

In this section we consider the general smooth integral operator

$$(\mathcal{K}\tau)(\mathbf{x}) = \int_{\partial\Omega} K(\mathbf{x},\mathbf{y})\tau(\mathbf{y})\,d\mathbf{y} \tag{18}$$

where we are integrating over the length of the boundary.

3.1 Nyström Method

In order to evaluate our integral operators numerically, we rely on the Nyström method of approximating the integral. This method discretizes the domain of the integral, and takes a weighted sum of the integrand at each point in the discretization.

$$\int_a^b h(t)\,dt \approx \sum_{i=1}^{N} w_i h(t_i) \tag{19}$$

Using the Nyström method, our integral operator (18) becomes

$$(\mathcal{K}\tau)(\mathbf{x}) \approx \sum_{i=1}^{N} w_i K(\mathbf{x},\mathbf{y}_i)\tau(\mathbf{y}_i) \tag{20}$$

where $\{\mathbf{y}_i\}_{i=1}^n$ lies on the boundary. Kress [9] describes in detail how the above discretization yield a convergent approximation as N is increased.

3.1.1 Periodic Trapezoid Rule

Now, consider BVPs where the domain has a smooth boundary. Let $\mathbf{y}(t)$ be a 2π periodic parameterization of this boundary. We can recast our boundary integral equation in terms of this parameterization as

$$\int_{\partial\Omega} K(\mathbf{x},\mathbf{y})\tau(\mathbf{y})\,d\mathbf{y} = \int_0^{2\pi} K(\mathbf{x},\mathbf{y}(t))\tau(\mathbf{y}(t))\frac{d|\mathbf{y}|}{dt}\,dt \tag{21}$$

Since the function $\mathbf{y}(t)$ is periodic over 2π, we can use the periodic trapezoid rule as a quadrature rule. That is if we discretize the domain of the integral into N points, we use

$$\begin{cases} t_k = \frac{2\pi k}{N} \\ w_k = \frac{2\pi}{N} \end{cases} \tag{22}$$

This quadrature rule is exponentially convergent for analytic functions ([9] 12.1). Thus the Nyström method is exponentially convergent if K is analytic in both variables. Using these nodes and weights, equation (19) becomes

$$\int_a^b h(t)\,dt \approx \sum_{i=1}^{N} \frac{2\pi}{N} h\Big(\frac{2\pi i}{N}\Big)$$

Now, we note that if we are trying to match conditions on the boundary, i.e. we are solving for τ in the equation

$$K\tau = f|_{\partial\Omega}$$

where f is gives the boundary data. Then we just need to solve the linear system

$$f(\mathbf{y}(t_i)) = \sum_{k=1}^{n} w_k K(\mathbf{y}(t_i), \mathbf{y}(t_k)) \frac{d|\mathbf{y}|}{dt}(t_k)\tau(\mathbf{y}(t_k)) \qquad \forall i = 0 \text{ to } n \tag{23}$$

Which we will denote

$$\mathbf{f} = \mathbf{A}\boldsymbol{\tau} \tag{24}$$

where

$$A_{i,j} = w_j K(\mathbf{y}(t_i), \mathbf{y}(t_j)) \frac{d|\mathbf{y}(t_j)|}{dt} \tag{25}$$

is an $N \times N$ matrix, and $\mathbf{f}_i = f(\mathbf{y}(t_i))$ and $\boldsymbol{\tau}_i = \tau(\mathbf{y}(t_i))$ are $N \times 1$ vectors. $\boldsymbol{\tau}$ is our unknown density function, as in (17)

Now, solving for $\boldsymbol{\tau}$ is a standard linear algebra problem. We can use $\boldsymbol{\tau}$ in equation (20) to approximate the desired function $(\mathcal{K}\tau)(\mathbf{x})$.

$$(\mathcal{K}\tau)(\mathbf{x}) \approx \sum_{i=1}^{N} w_i K(\mathbf{x}, \mathbf{y}(t_i)) \frac{d|\mathbf{y}|}{dt}(t_i)\boldsymbol{\tau}_i \tag{26}$$

3.2 Alpert Corrections

In the preceding sections, we have introduced the Nyström method of solving integral equations for a general smooth kernel K. Now, we wish to focus on the kernel $\Phi(\mathbf{x}, \mathbf{y})$ given by equation (8) which has a logarithmic singularity at the source $\mathbf{x} = \mathbf{y}$.

From equation (1) we have that $\Phi(\mathbf{x}, \mathbf{y}) = A(\mathbf{x}, \mathbf{y}) \log \frac{1}{\mathbf{r}} + B(\mathbf{x}, \mathbf{y})$. The main problem that we face using periodic trapezoid rule is that we must evaluate the fundamental solution at the singularity in order to fill the Nyström matrix $\mathbf{A}$ along the diagonal where $\mathbf{y}(t_i) = \mathbf{y}(t_j)$. In order to obtain a high-order convergent scheme for evaluating integral equations with a logarithmic singularity, we use Alpert corrections [1, 7].

If we have an underlying $N + 1$ node periodic trapezoid rule scheme, Alpert corrections will leave $N - 2a + 1$ nodes unaltered with the same weights. The a nodes to either side of the singularity are replaced with m nodes each, with positions and weights chosen using barycentric interpolation ([1] section 5 describes how to calculate these nodes and weights). These nodes will lie off the underlying periodic-trapezoid grid, with several nodes clustered near, but not lying on the singularity. We are then able to solve the system on these new nodes, and interpolate τ measured at these Alpert nodes to $\boldsymbol{\tau}$ using the original periodic trapezoid nodes.

This scheme has been proven to have $O(h^l \log(h))$ error convergence as $h \to 0$ ([1] Cor. 3.8) for functions of form (1), where $h = 2\pi/N$. The number of new nodes m on either side of the singularity is either l or $l - 1$ [7].

From [7], we see that choosing $a = 10, m = 15$ gives $l = 16$, which are the values that we used in our implementation. Note that this requires that $N > 2m$. We make these corrections on each row of the matrix, since we must integrate over each fundamental solution. Since we only need make $O(1)$ corrections per source, the total number of corrections made to our matrix $\mathbf{A}$ (eqn. (24)) is $O(N)$.

4 Fundamental Solution Evaluation

In order to fill the Nyström matrix required to numerically solve the integral equation, we first need to be able to numerically evaluate the fundamental solution (8). While we are able to write the fundamental solution as an integral along the real axis, the actual evaluation of this integral is difficult, and thus the discussion of this evaluation constitutes a large fraction of the work presented in this thesis.

4.1 Numerical Steepest Descent

From equation (8) we are given the following fundamental solution to the PDE $(\Delta + x_2 + E)u = 0$:

$$\Phi(\mathbf{x}, \mathbf{y}) = -\frac{1}{4\pi} \int_{-\infty}^{\infty} \exp i\big[\frac{|\mathbf{x}-\mathbf{y}|^2}{4} e^{-s} + (\frac{1}{2}x_2 + \frac{1}{2}y_2 + E)e^s - \frac{1}{12}e^{3s}\big]\, ds$$

On the real line the integrand oscillates between -1 and $+1$. The oscillations increase as $s \to -\infty$ due to the e^{-s} term and as $s \to +\infty$ due to the e^s and e^{3s} terms. This makes numerical evaluation of the integral on the real line infeasible.

However, the above integrand is entire (as it is a composition of exponentials, which are entire). Thus, we can deform the contour of integration off the real line into the complex plane in order to evaluate the function, and will obtain the same result as integrating along the real axis as long as the endpoints of the integral are the same.

This method is explained in detail in [2, 8]. For our purposes, we seek a contour that starts at $-\inf$ on the real axis, and ends at $+\inf$ in the real axis, while avoiding any regions of $\mathbb{C}$ that are exponentially large. When the integrand is oscillatory, this requires passing through stationary phase points.

Definition 3. *Given an integrand $f(s)e^{ig(s)}$, the stationary phase points are where $g'(s) = 0$.*

Figure 4 shows where the relevant stationary points of the integrand in (8) are located. We can steer the contour of integration through these stationary points from one exponentially small region of the integrand to the other. This allows us to evaluate the integrand only along a small region of the contour, as the integral over the contour excluding this region can be easily made to be less than machine precision.

4.2 Choosing a Contour

We make the following definitions to simplify (8):

$$a = \frac{|\mathbf{x}-\mathbf{y}|^2}{4}, \qquad b = \frac{1}{2}x_2 + \frac{1}{2}y_2 + E$$

So now the integral becomes

$$\int_{-\infty}^{\infty} \exp\left(i(ae^{-s} + be^s - \frac{1}{12}e^{3s})\right) ds \tag{27}$$

We construct a family of curves parametrized by a and b that avoid the exponentially large regions of the integrand. In order to do this, we find the stationary points

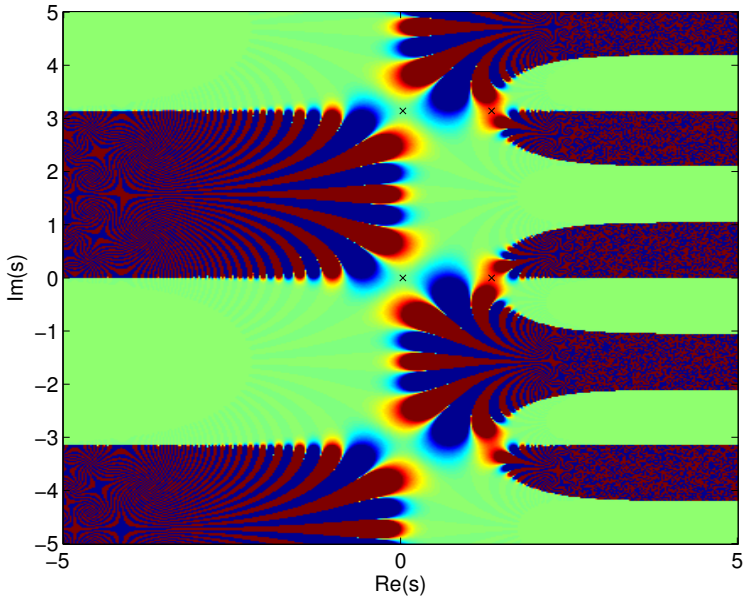

Figure 4: Integrand for $a = b = 4$. Stationary points are marked with `x`

for the integrand, which are centered in the calm regions of the integrand and serve as the gateways from one exponentially small region to another.

We find the stationary points for (27) as follows [11]

$$\begin{aligned}
\frac{d}{ds}[ae^{-s} + be^{s} - \frac{1}{12}e^{3s}] = 0 &\qquad \text{Definition 3}\\
-ae^{-s} + be^{s} - \frac{1}{4}e^{3s} = 0 &\\
\frac{1}{4}e^{4s} + be^{2s} - a = 0 &\qquad \text{multiplication by } e^{s}\\
e^{2s} = 2(b \pm \sqrt{b^2 - a}) &\qquad \text{quadratic formula}\\
e^{s} = \pm\sqrt{2(b \pm \sqrt{b^2 - a})} &\\
s = \log \pm\sqrt{2(b \pm \sqrt{b^2 - a})} &
\end{aligned}$$

Thus, for any branch of log, there are four stationary points:

$$\sigma_{stat} = \log \pm\sqrt{2(b \pm \sqrt{b^2 - a})}$$

For concreteness, let $\sigma_1 = \log\sqrt{2(b + \sqrt{b^2 - a})}$ and $\sigma_2 = \log\sqrt{2(b - \sqrt{b^2 - a})}$.

A family of contours that steers through these stationary points into exponentially small regions of the integrand is given by [11] and written as:

$$\gamma(t) = t + ig_{a,b}(t),$$

where

$$g_{a,b}(t) = \begin{cases} \frac{1}{3}\arctan(x) - \frac{\pi}{3} & : b \le \sqrt{a}, \mathrm{Im}(\sigma_2) \le -\pi/3 \\ (\mathrm{Im}(\sigma_2) + \frac{\pi}{3})\exp\left(-(t - \mathrm{Re}(\sigma_2))^2\right) + \frac{1}{3}\arctan(x) - \frac{\pi}{3} & : b \le \sqrt{a}, \mathrm{Im}(\sigma_2) \ge -\pi/3 \\ \left((\frac{1}{\pi} + \frac{1}{2})\arctan(2(t - \mathrm{Re}(\sigma_2) + \frac{w}{2})) - (\frac{\pi}{4} - \frac{1}{2})\right)\times & \\ \left((\frac{1}{\pi} + \frac{1}{6})\arctan(-4(t - \mathrm{Re}(\sigma_1) - \frac{v}{4})) - (\frac{\pi}{12} - \frac{1}{2})\right) & : \text{otherwise} \end{cases}$$

where in the last line $v = \tan(\frac{\pi^2 - 6\pi}{12+2\pi})$ and $w = \tan(\frac{\pi^2 - 2\pi}{4+2\pi})$.

These formulas are messy, but basic idea is to perturb the contour below the real axis, so the contour lies in exponentially small regions of the s-plane as it goes to $\pm\infty$, and steer through the stationary points with a bump shaped function. In figure 4, we see that there are multiple regions in which the integrand dies off as $s \to \pm\infty$. These correspond to different branch cuts of the integrand. Steering through the two regions directly below the real axis give us the desired result.

Note on Stationary Point Evaluation:
We wish for σ_2 to be continuous over the a, b plane. If we transition from a region where $b^2 - a$ is positive to a region where it is negative, the expression $b - \sqrt{b^2 - a}$ moves from the real line into the bottom-half of the complex plane. We have that

$$\sigma_2 = \log(\sqrt{2(b - \sqrt{b^2 - a})}) = \frac{1}{2}\log(2(b - \sqrt{b^2 - a}))$$

Since the quantity evaluated by the logarithm lies in the upper complex plane in the left-hand expression, and the lower-complex plane in the right hand expression, if the branch cut of the logarithm lies along the negative real axis (as is standard), the left and right hand expressions will disagree by $i\pi$. To ensure that σ_2 steers the contour into the correct region, we found that it was necessary to enforce $\mathrm{Im}(\sigma_2) < 0$

4.3 Evaluation in Different Regions

So far, we have chosen contours that steer into exponentially decaying regions of the integrand. Now, we consider evaluation depending on the form of the contour. We use the following shorthand to differentiate regions where the contour is chosen differently:

Region	Description
1	$b \le \sqrt{a}, \mathrm{Im}(\sigma_2) \le -\pi/3$
2	$b \le \sqrt{a}, \mathrm{Im}(\sigma_2) \ge -\pi/3$
3	$b > \sqrt{a}$

Table 1: evaluation regions of integrand

4.3.1 Regions 1 & 2

Regions 1 and 2 are both similar in that $\mathrm{Re}(\sigma_1) = \mathrm{Re}(\sigma_2)$ So there in only one maximum in the magnitude of the integrand when following the contour. Since the maximum

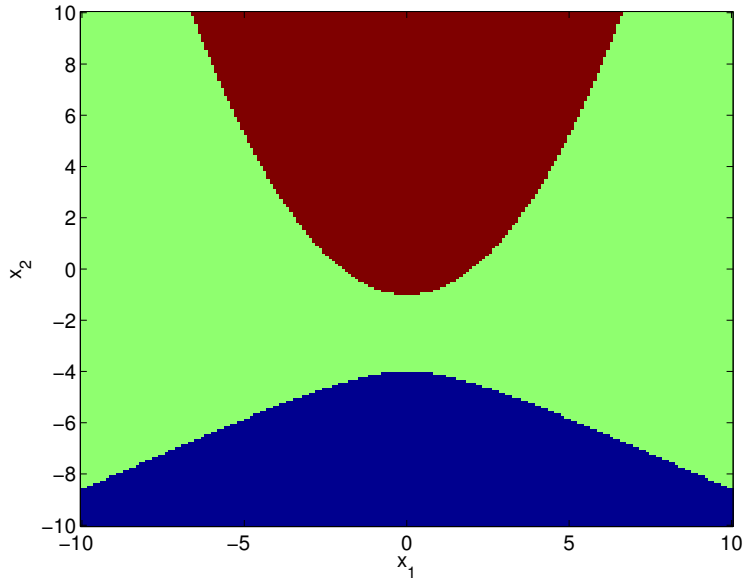

Figure 5: Different evaluation regions as described in table 1 in the x plane for $E = 1$, source at the origin. Blue corresponds to region 1. Green corresponds to region 2. Red corresponds to region 3.

magnitude of the integrand is given by $\mathrm{Re}(\sigma_1)$, our strategy for choosing bounds for quadrature points is to start at this point, and move along the contour in both directions until its magnitude dies off to below machine precision.

We do this by choosing a starting distance and multiplying it by a factor r repeatedly until the magnitude of the integrand dies to below machine precision. In the event that the starting distance is above machine precision, we decrease by dividing by r repeatedly until we find where the magnitude of the integrand rises above machine precision, and then use the most recent distance that was still below machine precision. We have found that setting $r = 1.2$ works well for obtaining reasonably tight bounds on this region of the integrand. Since this region is not symmetrical, we have to perform this process independently both on the right-hand and left-hand sides of the stationary point.

Once we have obtained bounds on the region where the magnitude of the integrand along the contour is above machine precision, we are able to use a constant number of quadrature points using trapezoid rule to evaluate the integral.

4.3.2 Region 3

Region 3 differs from regions 1 and 2 in that $\mathrm{Re}(\sigma_1) \neq \mathrm{Re}(\sigma_2)$. This means that there will be two local maxima of the magnitude of the integrand along the contour.

While the example in figure 8 looks relatively benign, care is needed when considering all possible cases. We can not simply find bounds on an evaluation regions by going left of the left-most stationary point and right of the right-most stationary point and use a constant number of evenly-spaced quadrature points in all cases. First, let us consider a high-energy case (so $b^2 >> a$ in certain cases).

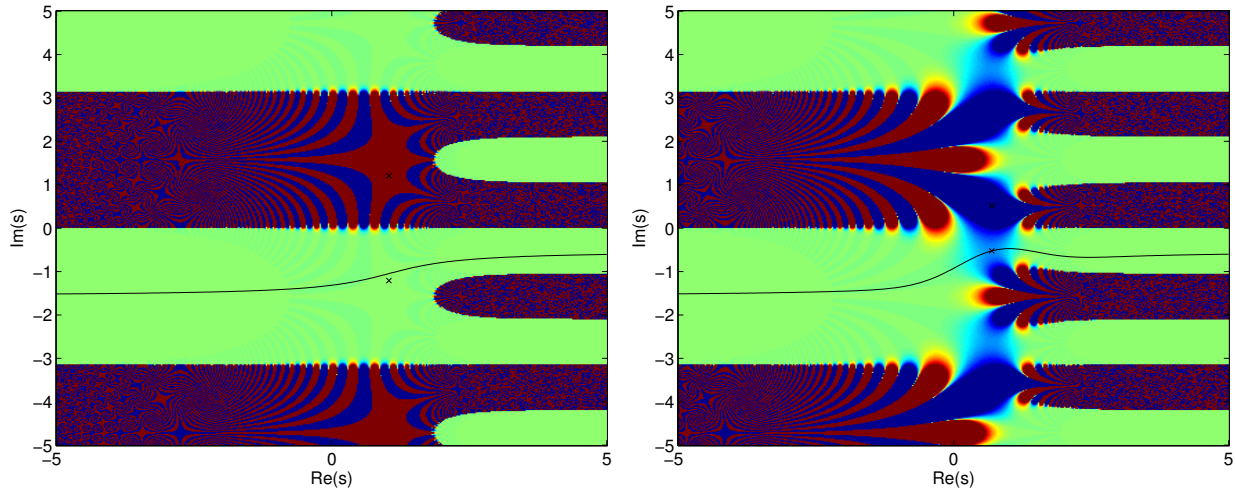

Figure 6: Left: Sample contour in evaluation region 1 ($a = 16, b = -3$). Right: Sample contour in evaluation region 2 ($a = 4, b = 1$)

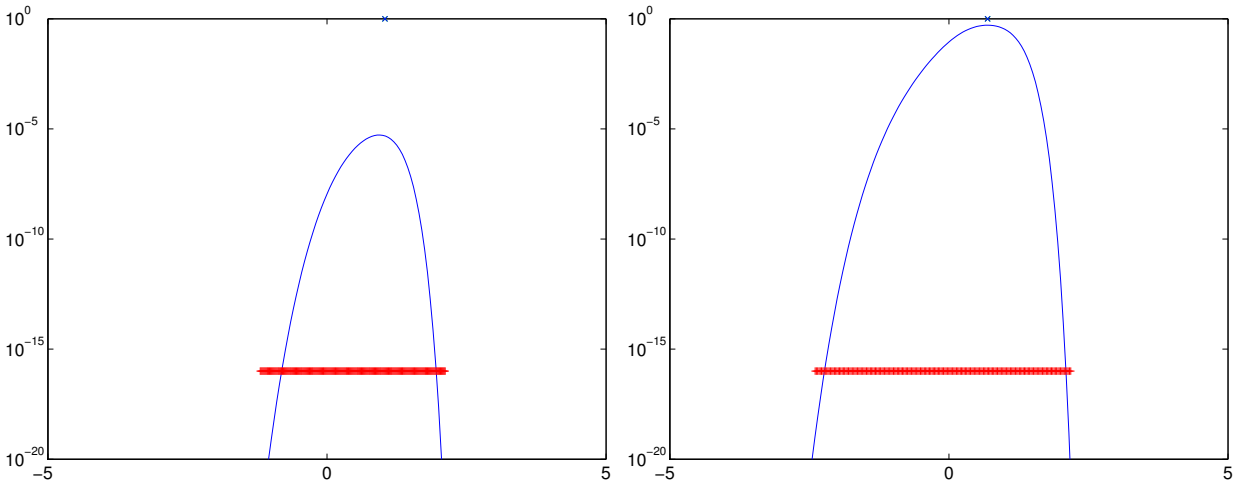

Figure 7: Left: magnitude of integrand along contour for $a = 16, b = -3$ which lies in region 1. Right: magnitude of integrand along contour for $a = 4, b = 1$. In both pictures, there is a blue `x` at the top of the frame corresponding to the real part of the stationary points. Red band is composed of `+`s indicating quadrature points. In both figures, the horizontal axis is the parameterization variable t, and the vertical axis the the magnitude of the integrand through the contour at that point.

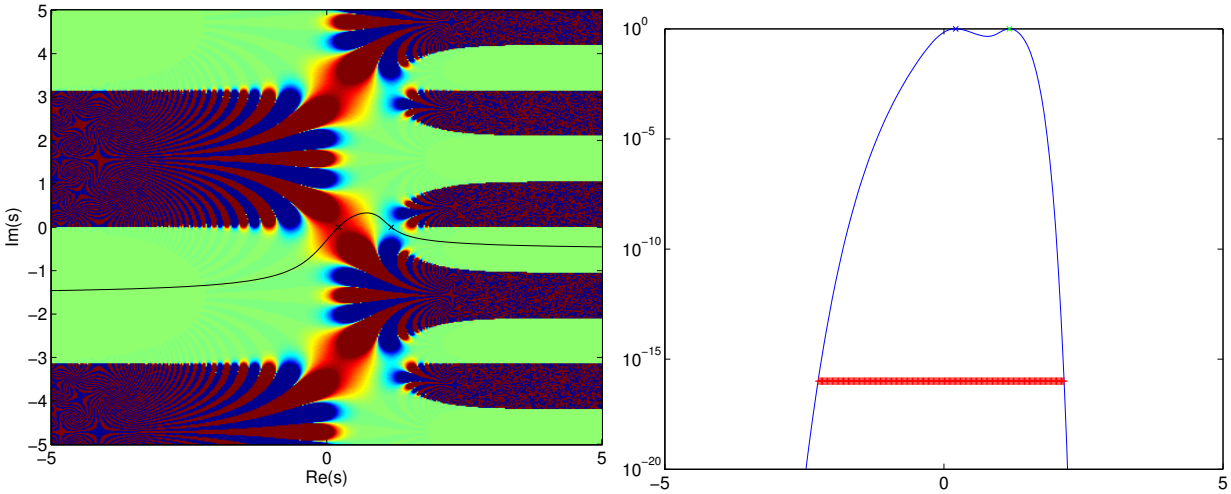

Figure 8: Left: Sample contour in evaluation region 3 ($a = 4, b = 3$). Right: magnitude of integrand along the same contour. The two `x`s at top are the locations of stationary points. The red band is composed of `+`s indicating quadrature points.

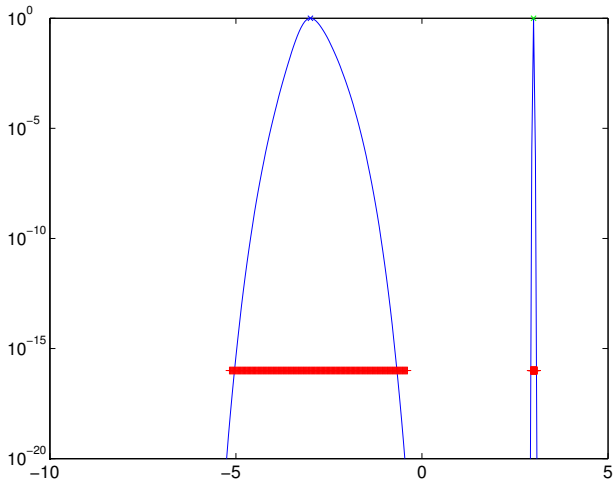

Figure 9: Magnitude of the integrand for $x_1 = 0, x_2 = 1, E = 100$ ($a = 0.25, b = 100.5$) along the chosen contour.

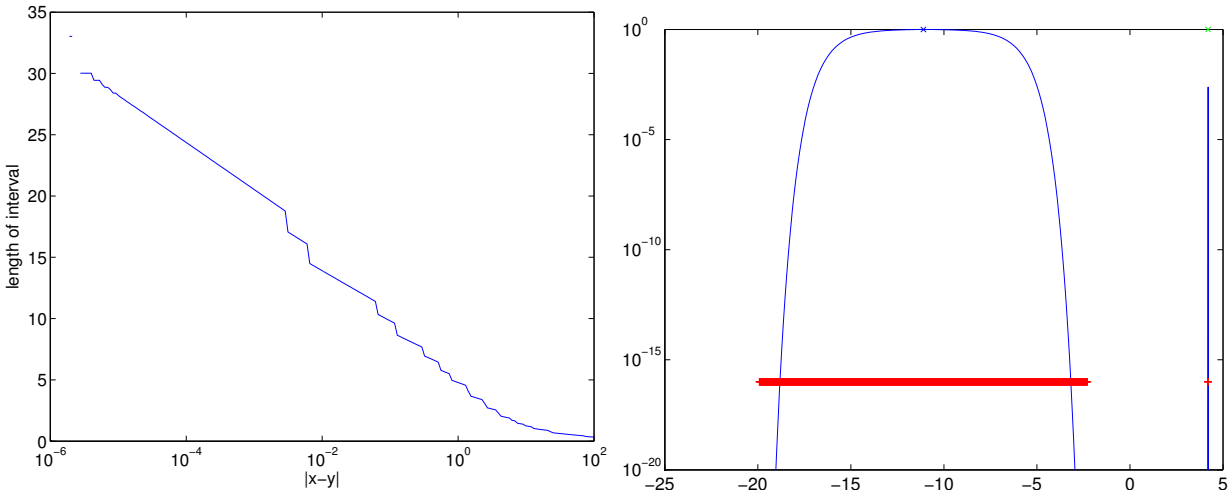

Figure 10: Left: Length of interval (as determined by find endpoints routine) where left-hand bump is greater than machine precision, as the evaluation point approaches the source along the x_2 axis. Contours are for $E = 100$. Right: Example contour for $x_1 = 0, x_2 = 10^{-3}, E = 100$

In this case, the magnitude of the integrand dies off to below machine precision along the contour between the two stationary points. To evaluate this integral, we can just treat both bumps separately using the same method as in regions 1 and 2 described above. To inform our starting distance for the width of each bump, we find the minimum of the integrand between the two stationary points. In this case, since the minimum is below machine precision, the upper bound for evaluation of the left-hand bump will only shrink, and the lower bound of the right-hand bump will only grow. This means that the evaluation regions will not intersect, so we can treat the two bumps as separate problems numerically. An example of this is shown in figure 9

In the case that the integrand does not die off to below machine precision between the stationary points, we can not treat the two bumps separately. In this case, we double the number of quadrature points and use them over the width of the interval containing both bumps. Although we are doubling the number of quadrature points, we are only evaluating over one interval, so this case does not take any longer than the preceding case, which evaluated over two intervals. An example of this is shown in figure 8.

One final regime that requires special consideration is the evaluation of points near the source. Since we assume that $E > 0$, we have that as $x \to 0$ that $a \to 0$ and $b \to E$. Thus $b^2 > a$ and we are in region 3.

As we see in figure 10, the width of the left-hand bump grows logarithmically as the source is approached. In order to compensate for this behavior, we scale the number of quadrature points used on the left-hand bump logarithmically, to ensure adequate resolution at the edges of the bump, where the magnitude of the integrand changes rapidly. The right-hand bump does not display such behavior, so we are able to maintain a constant number of quadrature points for its evaluation.

In the case where the integrand does not die off in the middle, it is sufficient to scale the total number of quadrature points logarithmically.

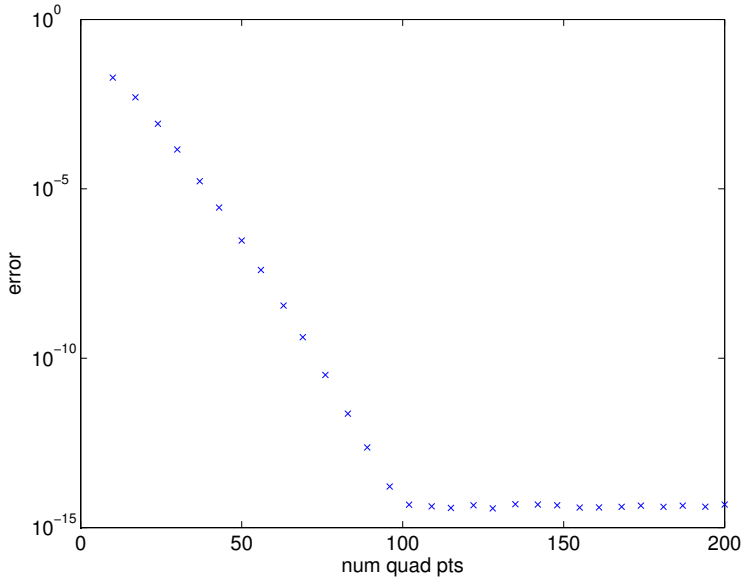

Figure 11: Convergence of 100 random points, $E = 1$, with radii in the interval $[1, 6]$ from the source (at the origin) as the number of quadrature points used to evaluate a bump is increased. Error is absolute error relative to a reference using 300 points, and is the supremum of errors over all points.

4.4 Accuracy of Fundamental Solution

There are two tests that we use to test the accuracy of our method of evaluating the fundamental solution. The first is a convergence test, which tests convergence of the fundamental solution to a particular value as the accuracy of quadrature is increased. The second test applies a finite-difference stencil to the fundamental solution to check agreement with the differential operator.

As seen in figure 11, our evaluation scheme converges exponentially to a value as the number of quadrature points is increased. We use $n = 200$ quadrature points in our evaluations, as convergence varies slightly for different values of a and b. Note that when close to the origin, the number of points used on the left-hand bump will increase logarithmically.

We can also test the accuracy of our solution by comparing to a finite-difference operator. The PDE we seek to satisfy is $(\Delta + x_2 + E)u = 0$ away from the source, so we can compare the result of an application of a finite-difference operator to the fundamental solution to 0. An example is shown in figure 12. Note that the convergence is best when the spacing on the finite difference operator is 10^{-4}, which is due to using a standard 5-point stencil of spacing h for Δ. By rounding error analysis, we expect optimal h is $\epsilon_{mach}^{1/3} \approx 10^{-5}$.

4.5 Derivatives

So far, we have seen evaluation for just the fundamental solution. However, we need knowledge of the derivatives (with respect to $\mathbf{y}$) in order to use the double layer operator. We find that

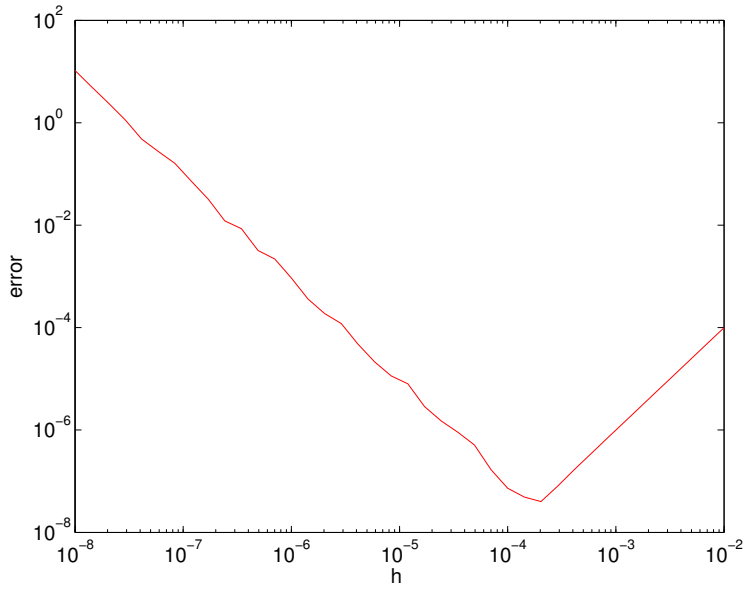

Figure 12: Agreement of 100 random points, $E = 1$, with radii in the interval $[1, 6]$ from the source with a finite-difference operator as a function of the spacing of the operator, h. Error displayed is the supremum over the error at all points. There are two sources of error: numerical error introduced from division by h^2 in the finite difference operator (dominates to the left of $h = 10^{-4}$), and error introduced from deviation of the function from its linear approximation (dominates to the right of $h = 10^{-4}$). $h = 10^{-4}$ is close to the place where the combination of these two sources of error is minimized.

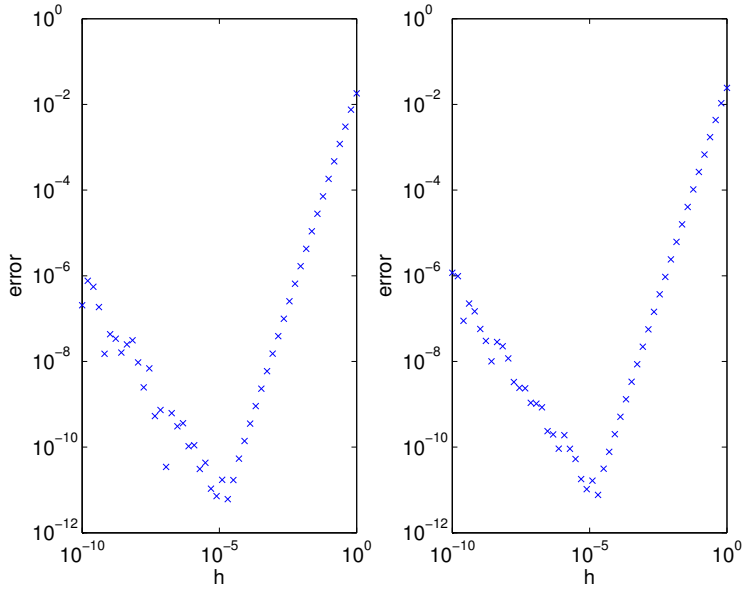

Figure 13: Accuracy of derivatives compared against finite-difference stencil of size h applied to fundamental solution. Data from $\mathbf{x} = (1, 2), \mathbf{y} = (0, 0)$, $E = 1$.

$$\Phi(\mathbf{x}, \mathbf{y}) = -\frac{1}{4\pi} \int_{-\infty}^{\infty} F(\mathbf{x}, \mathbf{y}, s)\, ds$$

Where

$$F(\mathbf{x}, \mathbf{y}, s) = \exp i\big[\frac{|\mathbf{x} - \mathbf{y}|^2}{4} e^{-s} + (\frac{1}{2}x_2 + \frac{1}{2}y_2 + E)e^{s} - \frac{1}{12}e^{3s}\big]$$

And straightforward calculation yields

$$\frac{\partial \Phi(\mathbf{x}, \mathbf{y})}{\partial y_1} = -\frac{1}{4\pi} \int_{-\infty}^{\infty} \frac{-i(x_1 - y_1)e^{-s}}{2} F(\mathbf{x}, \mathbf{y}, s)\, ds \tag{28}$$

$$\frac{\partial \Phi(\mathbf{x}, \mathbf{y})}{\partial y_2} = -\frac{1}{4\pi} \int_{-\infty}^{\infty} \frac{-i((x_2 - y_2)e^{-s} - e^{s})}{2} F(\mathbf{x}, \mathbf{y}, s)\, ds \tag{29}$$

So in either case, we are modifying the integrand by a pre-factor. To evaluate the above expressions, we can use the same contours as before (multiplication by e^s or e^{-s} will still allow the integrand to die off exponentially as desired). Thus, we can follow the same method as described above, simply modifying the integrand to agree with equations (28) and (29)

4.6 Implementation

Our original code was built and tested in a MATLAB environment. However, since each evaluation point requires a separate quadrature evaluation, and our routine to find endpoints for evaluation runs in a while-loop, there were several aspects of the code that were not able to take full advantage of MATLAB's vectorization capabilities. To speed up evaluation, we wrote a C function with a mex wrapper that allowed for faster

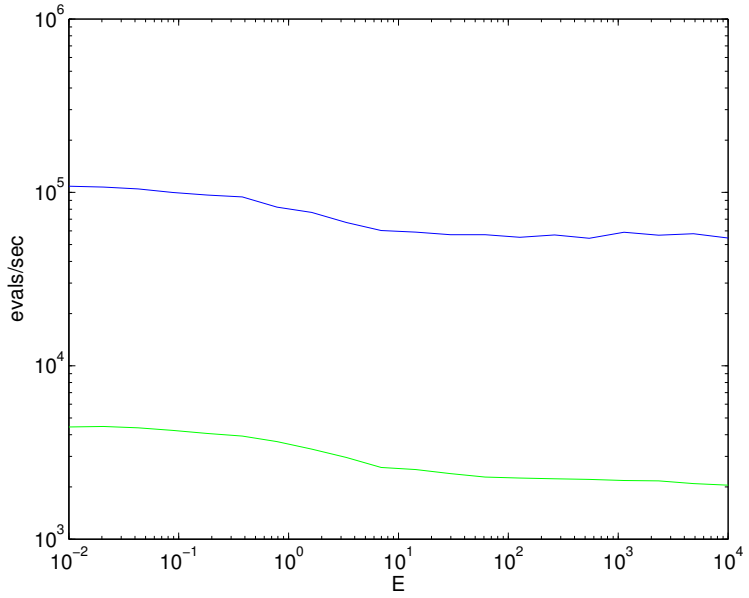

Figure 14: Speed of evaluation of the fundamental solution. Each data point was generated by evaluating the fundamental solution at 1000 randomly generated points in the annulus of outer radius 10, inner radius 1. Green: MATLAB code. Blue: mex function built on C code parallelized to 8 cores of a Xeon 3.3 GHz processor (16 threads).

for-loop and while-loop execution. An added benefit was the ability to parallelize the code using OpenMP. Since the evaluation time is dominated by performing hundreds of complex exponential evaluations for each target point, the code lends itself nicely to parallelization by partitioning the target points to be evaluated among processors.

As seen in figure 14 our method of evaluation has a lower bound of ≈ 3000 evaluations per second per thread regardless of E for points suitably far from the source of the fundamental solution. Since we grow the number of quadrature points logarithmically as we approach the source, evaluation time will also grow logarithmically.

As mentioned in section 4.4, we used 200 quadrature points per maximum in the integrand, increasing the number of points logarithmically as we approach the source. Note that this means that region 3 will be evaluated with twice as many quadrature points as regions 1 and 2, since it contains two maxima, and the other regions only contain one maximum. This accounts for the faster evaluation times for small E in figure 14, since more of the randomly chosen points lay in regions 1 and 2. For $E \geq 10$, all the points lay in region 3.

5 Results

In this section we explore numerical results of both interior, exterior, and scattering problems in two dimensions using the operator in equation (4), with Dirichlet boundary data. This corresponds to scattering off of a sound-soft obstacle [5].

5.1 Implementation

Numerical experiments were performed in a MATLAB environment.

Throughout our experiments, we used boundaries that can be described as a linear combination of Fourier modes of the circle. That is, if we center the domain at $\mathbf{p}$, we can parameterize the boundary as having radius

$$r(t) = \sum_{n=0}^{\infty} a_n \sin(nt) + b_n \cos(nt) \tag{30}$$

away from $\mathbf{p}$. Thus, $\partial\Omega$ lies on the curve

$$\mathbf{y}(t) = (r(t)\cos(t), r(t)\sin(t)) + \mathbf{p} \tag{31}$$

Our experiments generally take $\mathbf{p} = 0$.

We filled a Nyström matrix (25) $\mathbf{A}$ with kernel

$$K = \frac{1}{2} + D - \imath\eta S$$

with $\eta = \sqrt{E}$ for exterior/scattering problems and kernel

$$K = \frac{1}{2} - D$$

for interior problems. 16th order Alpert corrections were made along the diagonal of $\mathbf{A}$ using code modified from `MPSpack` [12].

After filling the boundary data vector, we then can simply solve for density $\boldsymbol{\tau}$ using backslash in MATLAB, if $N < 10^4$, or GMRES for larger matrices.

After finding $\boldsymbol{\tau}$, we can construct a numerical approximation to the solution $u = (K\tau)(x)$ as in equation (26).

5.2 Separation of Variables Solution

In this section, we derive a solution to the PDE (4) in order to check the accuracy of our solutions.

We can derive a solution for the PDE (4) by using separation of variables to obtain the ordinary differential equations

$$(\frac{\partial^2}{\partial x_1^2} + E)u_1 = 0$$

$$(\frac{\partial^2}{\partial x_2^2} + x_2)u_2 = 0$$

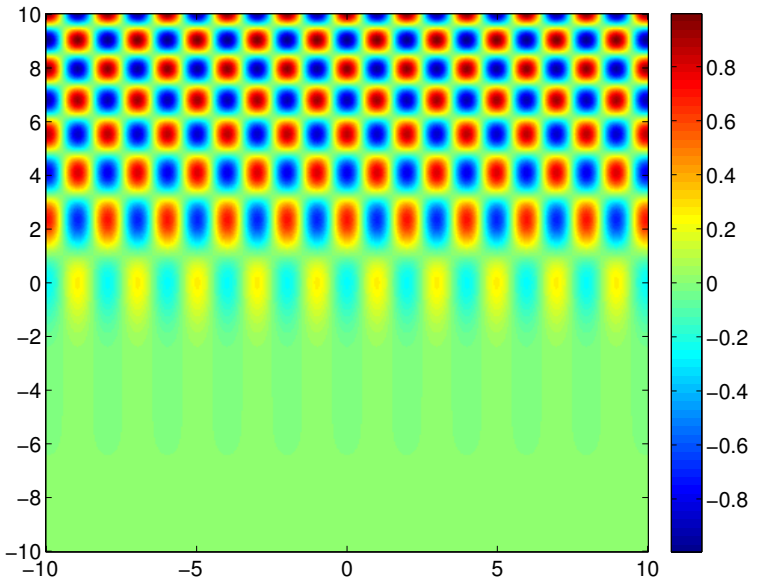

Figure 15: Left: a separation of variables solution for $E = 10$. Function is given by $\cos(\sqrt{10}x_1) \cdot Ai(-x_2)$

The solution to the first is just a sinusoid of wavelength $k = \sqrt{E}$, and the solution to the second is an Airy function. Thus, we can write a solution to (4) as

$$u(\mathbf{x}) = (a\cos(\sqrt{E}x_1) + b\sin(\sqrt{E}x_1)) \cdot (c \cdot Ai(-x_2) + d \cdot Bi(-x_2)) \tag{32}$$

where a, b, c, d are arbitrary constants and Ai, Bi are Airy functions of the first and second kinds, respectively.

5.3 Interior/Exterior Dirichlet Problems

We are able to test the accuracy of our integral equation formulation by using boundary data of a known solution to the PDE in the domain. For interior problems, we can use a of the form of equation (32). Alternatively, we can use a fundamental solution with the source outside the boundary of the domain. Both these options will satisfy the PDE inside the domain, so if we use boundary data generated by either of these functions into our integral equation formulation, we can test our ability to reconstruct the known solution.

Exterior problems require a radiative solution [5], so we can use a fundamental solution inside the boundary to generate boundary data. Again, this will enable us to compare our integral equation solution to the actual solution.

5.4 Scattering

Scattering problems are a subclass of exterior BVPs, and involve solving for the scattered field due to an incident wave hitting an object. Here, we consider "soft sound scattering" where the scattered field (u) cancels out the field of the incident wave (u^i)

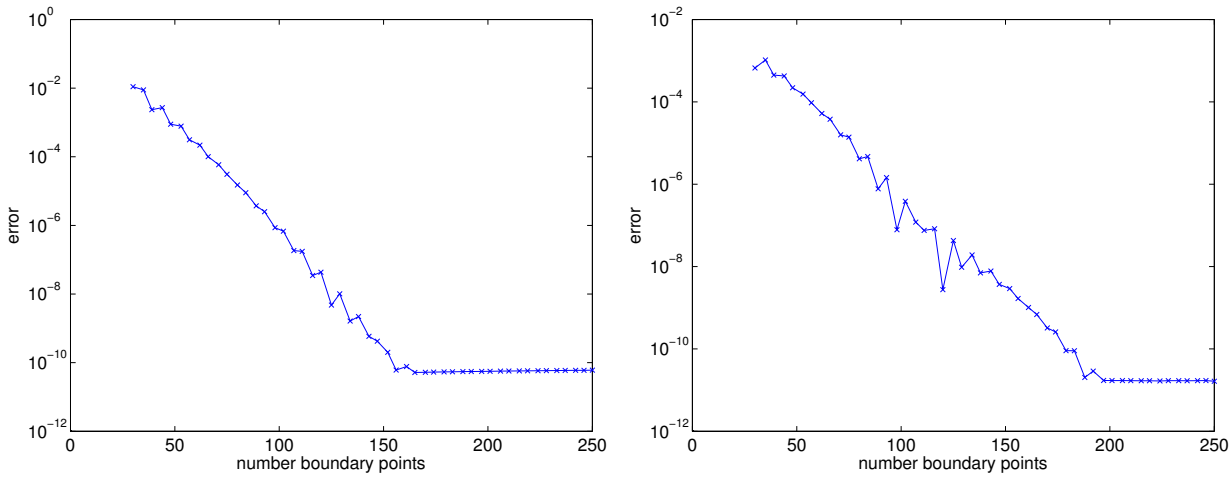

Figure 16: Left: convergence at 30 points to known solution to an interior BVP in the unit disk as the number of boundary nodes increases. Solution is $u = cos(x_1)Bi(x_2)$, where Bi is the Airy function of the second kind. Right: convergence at 30 points to a known solution to an exterior BVP outside the unit disk as the number of boundary nodes increases. Solution is the fundamental solution with its source at the origin, which is inside the boundary (not in the exterior domain). $E = 1$ in both figures.

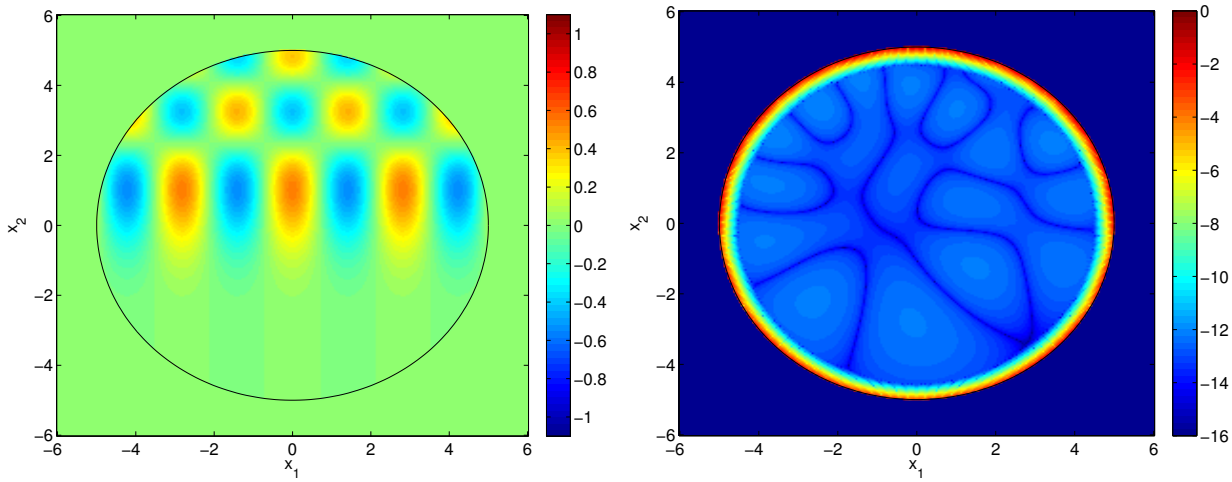

Figure 17: Left: interior problem with known solution $u = \cos(\sqrt{5}x_1) \cdot Ai(-x_2)$ in a disk of radius 5, $E = 5$. $N = 250$ boundary points were used. Note that error grows near boundaries, as convergence is point-wise, but not uniform in the domain.

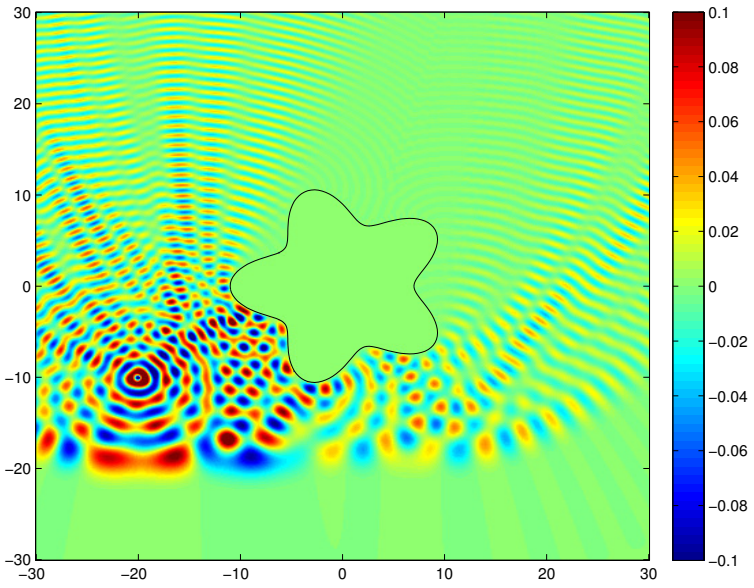

Figure 18: Combined field u^t for a scattering problem, $E = 20$, 200 boundary points used. The incident wave is from a point source located at $(-20, -10)$. Matrix fill time: 29.5 sec. Matrix solve time: 4.9×10^{-3} sec. Average time to construct the solution at each point was 0.128 sec.

on the boundary of the scatterer. In this case our integral formulation, using the combined field

$$(D + \frac{1}{2} - i\eta S)\tau = -u^i|_{\partial\Omega}$$

Which is approximated by the Nyström method by the linear system

$$\mathbf{A}\boldsymbol{\tau} = \mathbf{f}$$

We can then construct u from $\boldsymbol{\tau}$, as given by equation (26). The total field u^t is given by the sum of the incident wave and the scattered wave

$$u^t = u + u^i$$

As mentioned in the introduction, BIEs gain a significant advantage over standard discretization schemes in scattering. No extra steps are needed to ensure a radiative solution, as the radiation condition is automatically satisfied by the fundamental solution. Additionally, we have the option of evaluating u^t at only a few points, rather than solving for u^t in a large domain, which is the only option with standard discretization schemes.

Two examples of scattering problems are given in figures 18 and 19. In both figures, the scatterer was made to be $O(E)$ so that the wavelength changes significantly over the scatterer. Note how the waves bend parabolically around the scatterers. In both figures, waves die off below the classical limit ($x_2 = -30$ and -65 respectively).

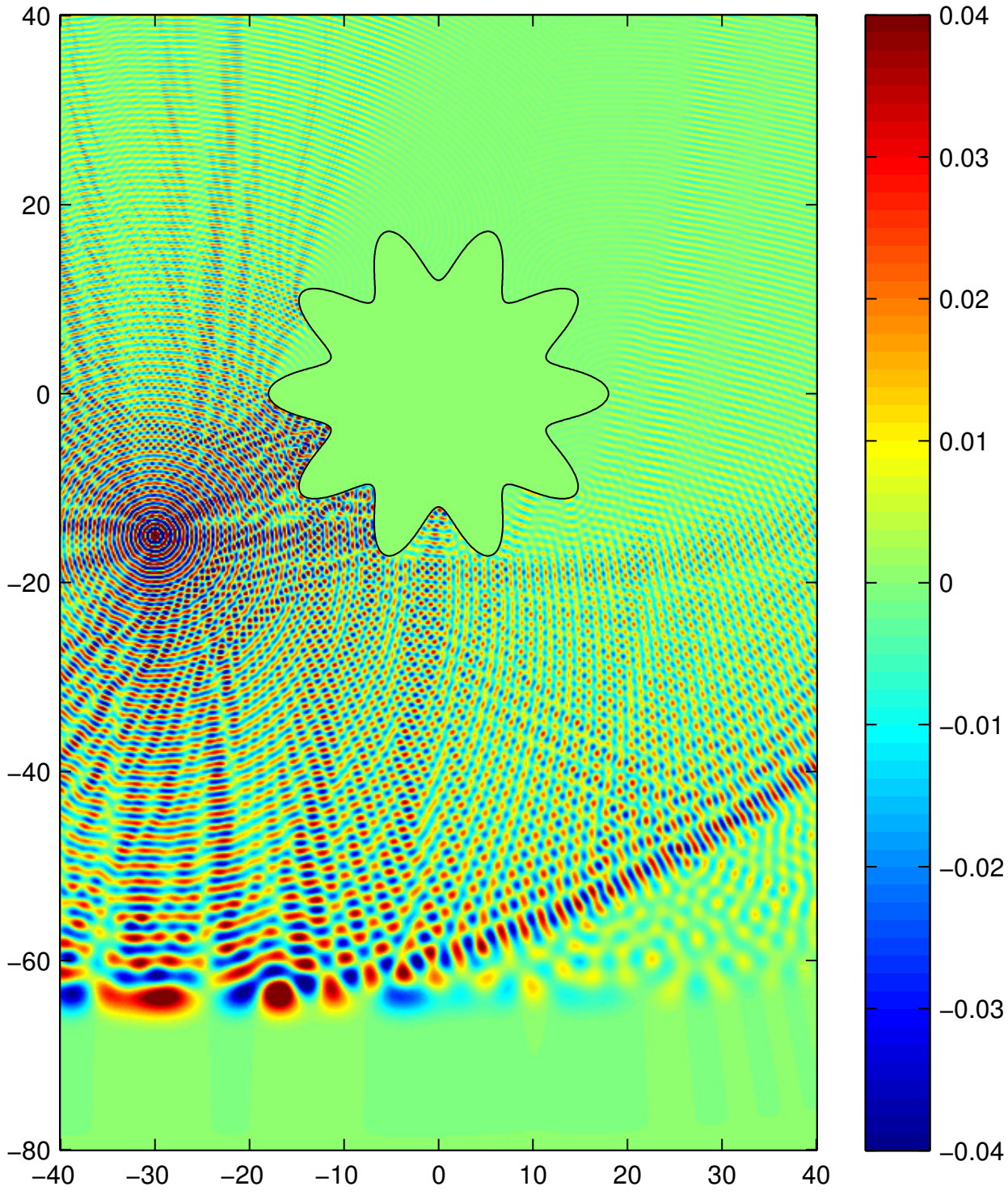

Figure 19: Combined field u^t for a scattering problem, $E = 65$, 1600 boundary points used. The incident wave is from a point source located at $(-30, -15)$. Matrix fill time: 343 sec . Matrix solve time: 0.24 sec. Average time to construct the solution at each point was 0.07 sec.

N	matrix fill time	matrix solve time	construction time	error
1000	184.8	0.0940	0.682	1.92e-7
1100	211.8	0.111	0.750	7.76e-8
1200	231.6	0.131	0.822	3.60e-8
1300	260.2	0.182	0.871	8.20e-9
1400	288.4	0.186	0.951	1.20e-9
1500	317.3	0.215	1.05	1.30e-10
1600	343.8	0.244	1.09	2.67e-11
1700	374.6	0.281	1.15	1.04e-11
1800	407.2	0.356	1.24	3.21e-12
1900	441.8	0.464	1.32	1.08e-12
2000	466.1	0.516	1.39	–

Table 2: Table for different runs of the problem in figure 19. Matrix fill time is the time needed to fill the matrix $\mathbf{A}$ (in seconds). Matrix solve time gives the time needed to solve the system $\mathbf{f} = \mathbf{A}\boldsymbol{\tau}$ in seconds. Construction time is the time it takes to construct the solution at one point using equation (26) in seconds. Error gives the supremum of the difference of the solution for a given N compared to the solution with $N = 2000$. Errors and reconstruction times were calculated at 50 random points in the annulus of inner radiums 19, outer radius 21 centered at the origin. In reconstructing the solution, these trials were small enough that parallelization was not used.

5.5 Direct Solver

One of the advantages of boundary integral equations is the ability to create a direct solver, which is able to solve many problems with the same geometry very quickly. This is useful if we wish to model the results of many different incident waves hitting a scatterer. Applications include modeling circuit designs to solving inverse problems using radar/sonar.

In this section, we will consider a direct solver in the context of scattering, although these principles can be used in interior problems or standard exterior problems. Let us consider the problem where we wish to find the total field at L different points $\{\mathbf{x}_i\}_{i=1}^{L}$ in Ω using M different incident waves, We solve the linear system

$$\mathbf{F} = \mathbf{AT}$$

where $\mathbf{A}$ is our $N \times N$ Nyström matrix, and $\mathbf{T}$ and $\mathbf{F}$ are both $N \times M$ matrices, in which each column corresponds to a different $\boldsymbol{\tau}$ and $\mathbf{f}$ in (24). After solving for $\mathbf{T}$, we now have the information needed to construct the total field at any location $\mathbf{x}$ using equation (26). Since we wish to evaluate the total field at fixed points for each trial, we can construct a $N \times L$ matrix $\mathbf{B}$ that describes the mapping from each $\boldsymbol{\tau}$ to the field at our set of L points:

$$\mathbf{B}_{i,j} = w_j K(\mathbf{x}_i, \mathbf{y}(t_j)) \frac{d|\mathbf{y}}{dt}(t_j) \tag{33}$$

We can then perform the computation

$$\mathbf{BT} = \mathbf{U}$$

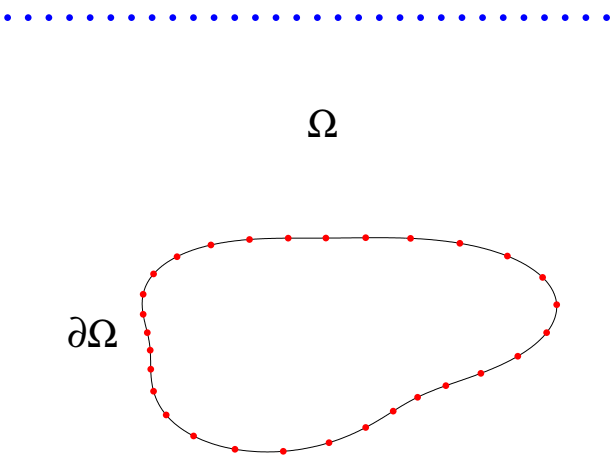

Figure 20: Example setup for direct solver. Red points are locations of sources of fundamental solutions. Blue points are evaluation points. Note that we can generally choose evaluation points to be anywhere in Ω.

Where $\mathbf{T}$ was computed above, and $\mathbf{U}$ is a $L \times M$, where each column $U_{i,j}$ is $u_j(\mathbf{x}_i)$, the scattered field at point $\mathbf{x_i}$ from the jth incident wave. We can then construct the total waves $U^t = U + U^s$.

	$\mathbf{A}$ construction	$\mathbf{B}$ construction	solve $\mathbf{F} = \mathbf{AT}$	multiply $\mathbf{BT} = \mathbf{U}$
N=1600, L=200	343 sec.	104.5 sec.		
M=20			1.14 sec	0.0112 sec
M=1			0.057 sec	$5.6 \times 10^{-3} sec$

Table 3: Direct solver setup, $E = 65$, same boundary as in figure 19, N = 1600 points. Incident waves were generated by point sources placed randomly outside the boundary. Note how once the $\mathbf{A}$ and $\mathbf{B}$ matrices are setup, performing a trial with a new incident wave is fast.

As seen in table 3, once the $\mathbf{A}$ and $\mathbf{B}$ matrices are computed, computing the scattered field using a different incident wave is very fast.

6 Conclusion

We have extended the use of boundary integral equations for the first time to Helmholtz boundary value problems in two dimensions where the square of the wavenumber varies linearly in one coordinate. We have presented a scheme for the numerical evaluation of the fundamental solution (8) first presented by Bracher et al. [3] that is accurate over the $\mathbf{x}$ plane, and for a wide range of E. While this scheme's speed is limited by the number of quadrature points used in evaluating each point, the scheme is readily parallelized, which allows for larger computations.

Using this fundamental solution, we have been able to solve boundary value problems where the wavelength changes significantly over the domain, including scattering problems with scatterers that are many wavelengths across. Our use of boundary integral equations in solving these problems offers significant advantages to the standard domain-discretization techniques.

References

[1] B. K. Alpert. Hybrid Gauss-trapezoidal quadrature rules. *SIAM J. Sci. Comput.*, 20:1551–1584, 1999.

[2] F. Bornemann and G. Wechslberger. Optimal contours for high-order derivatives. *IMA J. Numer. Anal.*, 33:403–412, 2013.

[3] C. Bracher, W. Becker, S. A. Gurvitz, M. Kleber, and M. S. Marinov. Three-dimensional tunneling in quantum ballistic motion. *Am. J. Phys.*, 66:38–48, 1998.

[4] D. Colton, R. Kress. Integral Equation Methods in Scattering Theory. John Wiley and Sons 1983.

[5] D. Colton, R. Kress. Inverse Acoustic and Electromagnetic Scattering Theory. Springer 1993.

[6] P. R. Garabedian Partial Differential Equations. AMS Chelsea Publishing, 1986.

[7] S. Hao, A. H. Barnett, P. G. Martinsson, and P. Young. High-order accurate methods for Nyström discretization of integral equations on smooth curves in the plane.

[8] D. Huybrechs and S. Vandewalle. On the evaluation of highly oscillatory integrals by analytic continuation. *SIAM J. Numer. Anal.*, 44:1026–1048, 2006.

[9] R. Kress. Linear Integral Equations. Springer 1989.

[10] R. J. LeVeque Finite Difference Methods for Ordinary and Partial Differential Equations SIAM, 2007.

[11] M. Mahoney. Unpublished notes, 2010.

[12] `MPSpack`: A MATLAB toolbox to solve Helmholtz PDE, wave scattering, and eigenvalue problems, Barnett A. H. and Betcke T. (2008–2013) `http://code.google.com/p/mpspack/`